Interfacing Differential Capacitive Sensors to Microcontrollers: A Direct Approach

Ferran Reverter and Òscar Casas, *Member, IEEE*

***Abstract*—This paper is a continuation of a previous work with regard to the direct connection of differential sensors to microcontrollers without using intermediate electronics between them. This paper focuses on the measurement of differential capacitive sensors, whereas the previous work dealt with the resistive counterparts. The proposed circuit is analyzed, and the main limitation seems to be the fact that the magnitude of the input parasitic capacitances of the microcontroller is similar to or even higher than the sensor capacitances. Methods to overcome this limitation are proposed, particularly when measuring low-value differential capacitive sensors such as microelectromechanical system (MEMS) sensors. Experimental tests of the circuit have been carried out by measuring a commercial capacitive accelerometer working as a tilt sensor. Although such a sensor has a low value (1.5 pF) and low sensitivity (0.105 pF/g), the measurement has shown a nonlinearity error of 1% full-scale span (FSS), which is a remarkable value considering the simplicity of the circuit.**

***Index Terms*—Accelerometer, capacitive sensor, differential capacitive sensor, microcontroller, sensor electronic interface, tilt sensor.**

I. Introduction

CAPACITIVE sensors are increasingly common in laboratory and industrial measurements to sense many physical and chemical quantities [1], [2]. They can be classified into two groups [2], [3]: 1) single capacitive sensors, which have only one sensing element, and 2) differential capacitive sensors (also known as push–pull half-bridge sensors), which have two sensing elements. The latter show inherent advantages: for instance, the effects of undesired inputs (e.g., temperature) equally affecting both sensing elements are cancelled. For this reason, differential capacitive sensors are widely used to measure acceleration [4]–[6], pressure, strain [7], linear and angular positions [8], [9], and displacement [10], [11].

Differential capacitive sensors usually have three parallel plates (the central plate being movable and the outer plates being fixed) and can be represented by two sensing capacitances (i.e., C_1 and C_2) with a common electrode, as shown in Fig. 1. At rest, the central plate is geometrically centered, and hence,

Manuscript received August 22, 2009; revised October 23, 2009; accepted October 24, 2009. Date of publication December 4, 2009; date of current version September 15, 2010. This work was supported by the Spanish Ministry of Education and Science and the European Regional Development Fund under Project DPI2006-04017. The Associate Editor coordinating the review process for this paper was Thomas Lipe.

The authors are with Instrumentation, Sensors and Interfaces Group, Castelldefels School of Technology, Universitat Politècnica de Catalunya, 08860 Castelldefels, Spain (e-mail: reverter@eel.upc.edu).

Color versions of one or more of the figures in this paper are available online at http://ieeexplore.ieee.org.

Digital Object Identifier 10.1109/TIM.2009.2036500

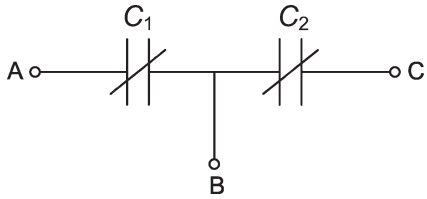

Fig. 1. Equivalent circuit of a differential capacitive sensor.

C_1 and C_2 are equal to the nominal value C_0. For a parallel-plate arrangement, C_0 is equal to

$$C_0 = \varepsilon_0 \varepsilon_r \frac{A_0}{d_0} \tag{1}$$

where ε_0 is the electric permittivity of vacuum, ε_r is the relative permittivity of the dielectric between plates, A_0 is the nominal area of the plates, and d_0 is the nominal distance between plates. In operation, however, the central plate of the sensor moves. Consequently, either the area or the distance between electrodes changes, and hence, both C_1 and C_2 change, but in opposite directions; such an effect can also be due to differential changes of permittivity, although these are less common. If the measurand changes the area, then C_1 and C_2 linearly change and can be expressed as

$$C_1 = C_0(1+x) \tag{2a}$$
$$C_2 = C_0(1-x) \tag{2b}$$

where x is the relative change of area due to the measurand. On the other hand, if the measurand changes the distance, then C_1 and C_2 hyperbolically change and can be expressed as

$$C_1 = \frac{C_0}{1-x} \tag{3a}$$
$$C_2 = \frac{C_0}{1+x} \tag{3b}$$

where x is the relative change of distance due to the measurand. Note that, if $x \ll 1$, then (3) can be approximated to (2). For both cases [(2) and (3)], the parameter x carries the measurand information and can be calculated by [10], [11]

$$x = \frac{C_1 - C_2}{C_1 + C_2} \tag{4}$$

whose value can range from -1 to 1.

Several electronic interfaces have been proposed and developed to measure differential capacitive sensors. Such circuits employ ac signals whose voltage [4], [7], [9], [11] or a time-related parameter [10], [12]–[15] is modulated by the differential sensor. In the former case, an ac signal coming from

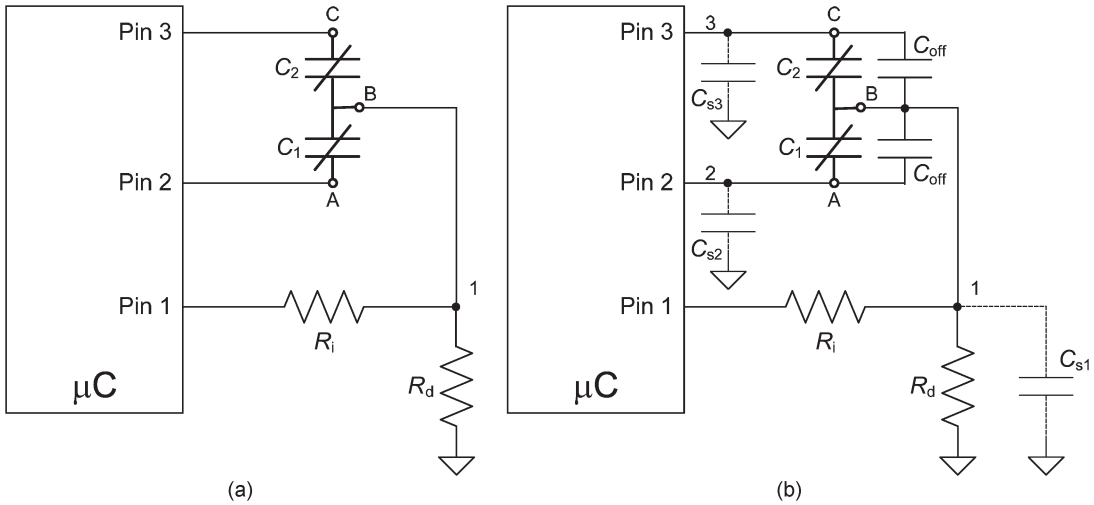

Fig. 2. (a) Direct interface circuit for a differential capacitive sensor. (b) Circuit in (a) when considering the parasitic capacitances.

an excitation source is applied to the sensor, thus resulting in an amplitude-modulated signal that is then demodulated and converted to digital by an analog-to-digital converter (ADC). In the latter case, the ac signal is generated by an oscillator or a similar circuit that includes the sensor, thus resulting in a time-modulated signal that can be connected to a digital processor (e.g., a microcontroller, μC) without the ADC. The preceding operating principles are also employed in commercial integrated circuits (ICs) specially designed to measure differential capacitive sensors, e.g., AD7745 (Analog Devices), MS3110 (Irvine Sensors), and UTI (Smartec).

To reduce the cost, complexity, area, and power consumption of sensor electronic interfaces, the concept of "direct interface circuit" was introduced in [16] and [17] and carefully analyzed in [18]. Direct interface circuits do not require either an intermediate signal conditioner (based on amplifiers or oscillators) or an ADC, but the sensor is directly connected to a general-purpose μC; actually, the analog front end is just a Schmitt-trigger (ST) buffer (embedded into the μC) that triggers a digital timer. A previous work [19] reported that direct interface circuits can satisfactorily measure differential resistive sensors, e.g., errors in the range of 0.01% full-scale span (FSS) and an effective resolution of 13 bits. This is due to the fact that uncertainty sources (e.g., the mismatch of the internal resistances of the port pins of the μC) are much lower than the sensor resistances (e.g., 1 kΩ). Another previous work [20] introduced a direct interface circuit for differential capacitive sensors, but it did not analyze nor optimize the circuit to measure low-value differential capacitive sensors (e.g., a few units of picofarads), which seems to be the usual case [4]–[6], [10]–[12], [15]. Accordingly, this paper extends the work done in [20], analyzes the limitations of the circuit when measuring low-value sensors, and proposes new measurement methods to overcome its limitations.

II. Operating Principle

The proposed direct interface circuit for differential capacitive sensors is shown in Fig. 2(a), which, as in [19], relies on measuring the discharging time of several RC circuits using a timer embedded into the μC. The sensor is modeled by the equivalent circuit shown in Fig. 1, R_i is a charging resistor, and R_d is a discharging resistor. Unlike the measurement of single capacitive sensors [18], the circuit in Fig. 2(a) does not include any reference capacitor.

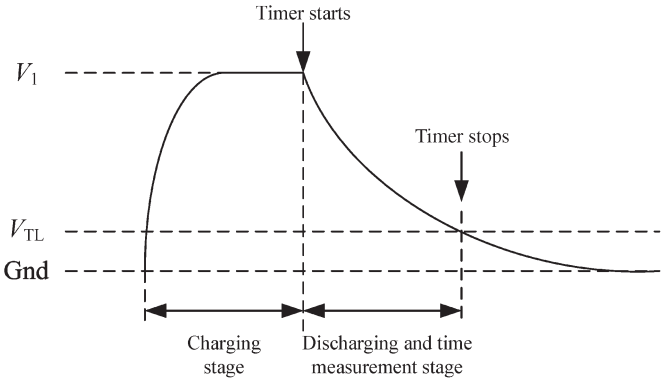

Fig. 3. Waveform of the voltage across R_d (Fig. 2) during the charge–discharge process.

The circuit in Fig. 2(a) works as follows. First, pin 1 provides a digital "1" (with an analog output voltage V_1), and then, the equivalent capacitance $C_{\rm eq}$ between Node 1 and ground (which is determined by the state of pins 2 and 3) is charged toward V_1 through R_i for a time interval longer than $5R_iC_{\rm eq}$; the effects of R_i in steady state can be assumed negligible whenever $R_i \ll R_d$. Once $C_{\rm eq}$ is charged to V_1, pin 1 is set as a high-impedance (HZ) input, and pins 2 and 3 do not change their state. At this instant, the timer starts, and $C_{\rm eq}$ is discharged toward ground through R_d. Then, when the discharging exponential signal (Fig. 3) reaches the lower threshold voltage $V_{\rm TL}$ of the ST buffer embedded into pin 1, the timer stops. The time interval needed to discharge $C_{\rm eq}$ from V_1 to $V_{\rm TL}$ through R_d is

$$T = R_d C_{\rm eq} \ln \frac{V_1}{V_{\rm TL}} \tag{5}$$

which is proportional to $C_{\rm eq}$. The timer converts T to a digital number using a high-frequency clock signal (whose period is equal to T_s) as a reference.

TABLE I
STATE OF PINS 2 AND 3 (FIG. 2), IDEAL AND ACTUAL EQUIVALENT CAPACITANCES $C_{\rm eq}$, AND RESULTING DISCHARGING TIME FOR EACH OF THE THREE MEASUREMENTS, WHERE $k_c = R_d \ln(V_1/V_{\rm TL})$

Meas.	Pin 2	Pin 3	Ideal Ceq	Actual Ceq	Discharging time
1	"0"	HZ	$C_{\rm eq1} = C_1$	$C_{\rm eq1} = C_{s1} + C_1 + C_{\rm off} + \dfrac{(C_2 + C_{\rm off})C_{s3}}{C_2 + C_{\rm off} + C_{s3}}$	$T_1 = k_c C_{\rm eq1}$
2	HZ	"0"	$C_{\rm eq2} = C_2$	$C_{\rm eq2} = C_{s1} + \dfrac{(C_1 + C_{\rm off})C_{s2}}{C_1 + C_{\rm off} + C_{s2}} + C_2 + C_{\rm off}$	$T_2 = k_c C_{\rm eq2}$
3	"0"	"0"	$C_{\rm eq3} = C_1 + C_2$	$C_{\rm eq3} = C_{s1} + C_1 + C_2 + 2C_{\rm off}$	$T_3 = k_c C_{\rm eq3}$

Using the previous operating principle, the circuit in Fig. 2(a) performs three discharging-time measurements: 1) measurement 1, which is dedicated to measure C_1; 2) measurement 2, which is dedicated to measure C_2; and 3) measurement 3, which is dedicated to measure C_1 plus C_2. Table I summarizes the state of pins 2 and 3, the ideal equivalent capacitance $C_{\rm eq}$, and the discharging time (T_1, T_2, and T_3) for each of the three measurements, where $k_c = R_d \ln(V_1/V_{\rm TL})$. Assuming the linear behavior described by (2), the discharging times in Table I can be expressed as

$$T_1 = k_c C_0 + k_c C_0 x \tag{6a}$$

$$T_2 = k_c C_0 - k_c C_0 x \tag{6b}$$

$$T_3 = 2k_c C_0 \tag{6c}$$

which shows that T_1 increases with x, T_2 decreases with x, and T_3 is insensitive to x. Ideally, from (6), T_3 is equal to T_1 plus T_2, and hence, its measurement could seem unnecessary. However, as will be shown in Section III, T_1 plus T_2 is more sensitive to both x and the parasitic capacitances than T_3. Accordingly, we propose the following time-based equation to estimate x:

$$x^* = \frac{T_1 - T_2}{T_3}. \tag{7}$$

Replacing (6) in (7) easily shows that the estimated value x^* is equal to the relative change x of the sensor.

According to (6), the discharging time depends on the parameter k_c, and hence, it depends on R_d, V_1, and $V_{\rm TL}$; these parameters can drift, for example, with temperature and/or time. However, according to (7), the estimated value x^* is independent of k_c (and, hence, of R_d, V_1, and $V_{\rm TL}$), provided that its value is the same for the three measurements. Therefore, the drifts of R_d, V_1, and $V_{\rm TL}$ are autocalibrated by the interface circuit itself. Furthermore, since the ratio $V_1/V_{\rm TL}$ is independent of the supply voltage $V_{\rm DD}$ of the μC, the drifts of $V_{\rm DD}$ are also autocalibrated.

III. ERROR ANALYSIS

The parasitic components of the circuit (particularly those related to the μC) can bring about an error in the estimation of x. Since the circuit is intended for capacitive sensors, the parasitic capacitances of the circuit seem to be the main source of error, and for this reason, their effects are analyzed next. Other parasitic components (such as the input and output resistances, and the input leakage current of the port pins of the μC) are expected to have less influence on the measurement. The effects of quantization and trigger noise affecting the discharging-time measurement are also analyzed in the following sections.

A. Effect of Parasitic Capacitances

Fig. 2(b) shows the circuit in Fig. 2(a) when considering the parasitic capacitances C_{s1}, C_{s2}, and C_{s3} between nodes 1, 2, and 3 and ground, respectively. The capacitance C_{s1} basically depends on the layout of the circuit, whereas C_{s2} and C_{s3} (which are expected to be very similar) are mainly due to the input parasitic capacitance of the port pin of the μC, which is about 8–10 pF. Note that this circuit is intended for nonremote sensors, and for this reason, no account is taken of the parasitic capacitances of the interconnecting cables. The circuit in Fig. 2(b) also includes a capacitance $C_{\rm off}$ in parallel with the sensor capacitances (i.e., C_1 and C_2) that is the sum of the following contributions: the passive capacitance $(C_{\rm off,1})$ of the sensor itself, the parasitic capacitance $(C_{\rm off,2})$ between the connecting tracks, and an offset capacitor $(C_{\rm off,3})$ intentionally added to the circuit, whose benefits will be explained later in this paper.

Table I (fifth column) shows the actual equivalent capacitance for the three discharging-time measurements when considering the circuit in Fig. 2(b). Assuming $C_{s2} = C_{s3} = C_s$ and $x \ll 1$, the resulting discharging times are

$$T_1 \approx k_c \left(C_0 + C_{s1} + C_{\rm off} + \frac{(C_0 + C_{\rm off})C_s}{C_0 + C_{\rm off} + C_s} \right) + k_c C_0 k_{s1} x \tag{8a}$$

$$T_2 \approx k_c \left(C_0 + C_{s1} + C_{\rm off} + \frac{(C_0 + C_{\rm off})C_s}{C_0 + C_{\rm off} + C_s} \right) - k_c C_0 k_{s1} x \tag{8b}$$

$$T_3 = 2k_c (C_0 + C_{\rm off} + C_{s1}/2) \tag{8c}$$

where $k_{s1} = m/(1+m)$, m being $(C_0 + C_{\rm off})/C_s$. According to (6) and (8), the parasitic capacitances increase the offset component (i.e., the value for $x = 0$) of T_1 and T_2 and the value of T_3, and they decrease the sensitivity to x by a factor of k_{s1}, which ranges from 0 to 1 and is represented in Fig. 4. Sensors with a high value of C_0 (e.g., tens or hundreds of picofarads) probably have $(C_0 + C_{\rm off}) \gg C_s$, which means a high value of both m and k_{s1} (i.e., k_{s1} tends to 1). However, sensors with a low value of C_0 (e.g., units of picofarads) probably have $(C_0 + C_{\rm off}) < C_s$, which means a low value of both m and

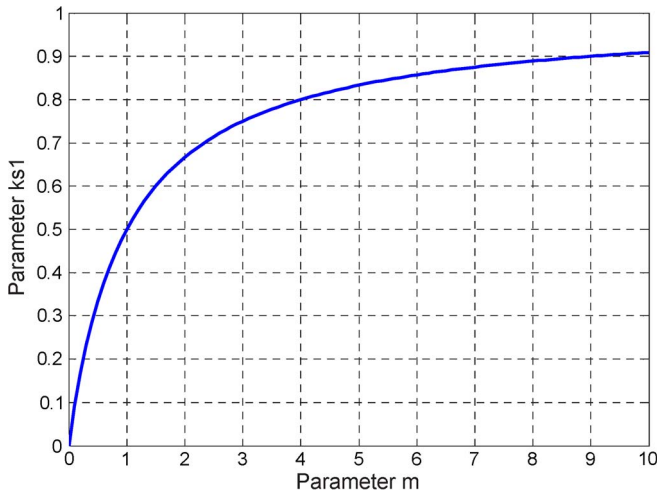

Fig. 4. Loss of sensitivity (represented by k_{s1}) versus the parameter m, which is equal to $(C_0 + C_{\text{off}})/C_s$.

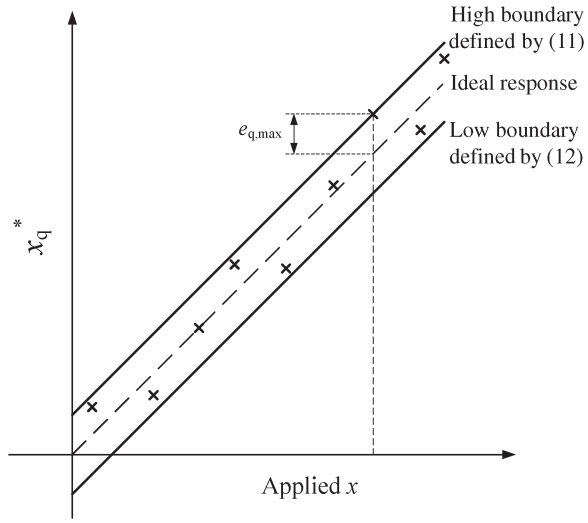

Fig. 5. Quantization effects on the estimation of x.

k_{s1}; in other words, if C_0 is low, then the measurement of C_1 (or C_2) is sensitive to C_2 (or C_1), and therefore, the discharging time T_1 (or T_2) is less sensitive to x. The loss of sensitivity of T_1 and T_2 (and, hence, of the difference $T_1 - T_2$) can also be quite critical in terms of resolution, because it reduces the range of digital numbers of the difference $T_1 - T_2$ to be calculated by (7).

The loss of sensitivity due to the parasitic capacitances can be improved by 1) avoiding high values of C_s and 2) increasing the value of C_{off}. With regard to the former, the port pins of the μC involved in the measurement should not be close to the ground plane. In relation to the latter, an additional capacitor $C_{\text{off},3}$ can be placed in parallel with C_1 and C_2. According to Fig. 4, it seems suitable to increase C_{off} so that $(C_0 + C_{\text{off}}) \approx 5C_s$, thus achieving $k_{s1} \approx 0.85$; higher values of C_{off} do not bring about a significant increase of k_{s1}. Regrettably, if the value of C_{off} increases, then, from (8), the offset component of T_1 and T_2 and the value of T_3 are higher.

Replacing (8) in (7) yields the value of x estimated due to the parasitic capacitances, i.e.,

$$x_c^* = x\frac{k_{s1}}{k_{s2}} \tag{9}$$

where $k_{s2} = 1 + (C_{\text{off}}/C_0) + (C_{s1}/2C_0)$. According to (9), parasitic capacitances bring about a gain error (determined by k_{s1} and k_{s2}), but not a nonlinearity error at least for $x \ll 1$. For sensors with a high value of C_0, the value of k_{s2} can be approximated as 1, i.e., the ideal value. However, for sensors with a low value of C_0, the value of k_{s2} can be somewhat greater than 1. If, in addition, the value of C_{off} is intentionally increased, then k_{s2} is even greater and whose value can be approximated to C_{off}/C_0. In such conditions, it seems appropriate to add a correction factor (CF) in (7), i.e.,

$$x^* = \frac{T_1 - T_2}{T_3} \cdot \text{CF} \tag{10}$$

where $\text{CF} = (k_{s2}/k_{s1}) \approx ((C_s + C_{\text{off}})/C_0)$, and its value can be estimated using the nominal or typical values of C_s, C_{off}, and C_0.

B. Effect of Quantization

The conversion of the discharging time (T_1, T_2, or T_3) to a digital number suffers from quantization effects that limit both the resolution and the accuracy of the measurement [19]. On the one hand, changes of the discharging time to be measured smaller than T_s are not detected by the digital timer, and on the other hand, any measured discharging time has a quantization error that ranges from $-T_s$ to 0 when using an input associated with a capture module. This error in the discharging-time measurement brings about an error in the estimation of x. Based on (7) or (10), here are the worst cases.

1) When T_2 and T_3 suffer from the maximum quantization error (i.e. $-T_s$), whereas T_1 suffers from the minimum one (i.e., zero). In such a case, when (10) is applied, the value of x estimated due to quantization is

$$x_q^* = \frac{T_1 - (T_2 - T_s)}{T_3 - T_s} \cdot \text{CF} \approx x + \frac{T_s}{2R_dC_0 \ln \frac{V_1}{V_{\text{TL}}}} \frac{1}{k_{s1}} \tag{11}$$

which is higher than the x applied.

2) When T_2 and T_3 suffer from the minimum quantization error (i.e., zero), whereas T_1 suffers from the maximum one (i.e., $-T_s$). Here, the result is

$$x_q^* = \frac{(T_1 - T_s) - T_2}{T_3} \cdot \text{CF} = x - \frac{T_s}{2R_dC_0 \ln \frac{V_1}{V_{\text{TL}}}} \frac{1}{k_{s1}} \tag{12}$$

which is lower than the x applied.

Fig. 5 shows the high and low boundaries defined by (11) and (12), respectively, of the response x_q^* versus x. Due to quantization effects, x_q^* can take any value between the boundaries, and consequently, the measurement of x can undergo zero, gain and/or nonlinearity errors. Let us proceed to quantify the nonlinearity error due to quantization, which is the main source of inaccuracy when a two-point field calibration is applied. Assuming that the values of x_q^* are randomly distributed between the boundaries (for example, see the crosses in Fig. 5), then the best-fit straight line is approximately the ideal response. In

such a case, the maximum nonlinearity error due to quantization expressed as a part of FSS is

$$\mathrm{NLE}_q = \frac{e_{q,\max}}{x_{\max} - x_{\min}} \cdot 100 \tag{13}$$

where

$$e_{q,\max} = \frac{T_s}{2R_d C_0 \ln \frac{V_1}{V_{\mathrm{TL}}}} \frac{1}{k_{s1}} \tag{14}$$

where $x_{\max}$ and $x_{\min}$ are the maximum and minimum values, respectively, of x applied. From (14), the nonlinearity error decreases when T_s decreases and/or R_d increases. High values of k_{s1} (i.e., values close to 1) are also appropriate in terms of linearity.

C. Effect of Trigger Noise

The discharging-time measurement explained in Section II relies on a voltage-threshold crossing, and hence, it is sensitive to noise. Noise can erroneously trigger the voltage comparison between the discharging exponential signal and the threshold voltage V_{TL} (Fig. 3), and therefore, the stopping point can be at the wrong time instant. Consequently, the discharging-time measurement can show a trigger time error that can limit the resolution of the measurement. For Gaussian noise, the probability density function of such an error is also Gaussian with the following RMS value [21]:

$$e_{\mathrm{trigger}} = \frac{\sqrt{E_{\mathrm{ni}}^2 + E_{\mathrm{ns}}^2}}{\mathrm{SR}} \tag{15}$$

where E_{ni} is the RMS noise voltage superimposed on V_{TL}, E_{ns} is the RMS noise voltage superimposed on the discharging exponential signal, and SR is the slew rate of the discharging exponential signal at the trigger point, which is equal to $V_{\mathrm{TL}}/(R_d C_{\mathrm{eq}})$. Note that the use of $C_{\mathrm{off},3}$ (to avoid the loss of sensitivity explained in Section III-A) reduces the value of SR, and hence, it increases trigger noise effects. The magnitude of E_{ni} and E_{ns} is not specified on μC data sheets since it depends on several factors, as explained in the following discussion.

Both the threshold voltage and the discharging exponential signal are generated from the supply voltage of the μC, and therefore, noise/interference superimposed on the supply voltage couples to them [22]. To reduce this noise and its effects, the μC must have a decoupling capacitor between the power supply pins and an appropriate layout of the ground and supply tracks. Furthermore, noise/interference rejection can significantly be improved by means of the resistor R_i (Fig. 2); this resistor decreases the cutoff frequency of the low-pass filter during the charging stage, and hence, the discharging exponential signal starts from a "clean" point [22]. Another source of noise affecting both the threshold voltage and the discharging exponential signal is that resulting from the μC activity, which is called software-related noise [23]. To decrease this noise and its effects, the μC should not execute instructions during the discharging stage, which can be achieved by placing the CPU of the μC into sleep mode [23]; software-related noise will be minimal if there is no CPU activity. The effects of trigger noise (but not those of quantization) can also be reduced by using the mean of N measurements as an estimate, thus reducing the RMS trigger time error by a factor of $\sqrt{N}$ [21], but, of course, at the expense of a longer measuring time.

TABLE II
FEATURES OF THE SINGLE-AXIS ACCELEROMETER USED TO TEST THE INTERFACE CIRCUIT IN FIG. 2

Feature	Min.	Typical	Max.	Units
Measuring range		± 2		g
Sensor capacitance (C_0)	1.2	1.5	1.8	pF
Passive capacitance ($C_{\mathrm{off},1}$)	0.8	1.0	1.2	pF
Sensitivity (of C_1 and C_2)	0.065	0.105	0.200	pF/g
Capacitance imbalance	-0.4	0.0	0.4	pF

IV. MATERIALS AND METHOD

The interface circuit shown in Fig. 2 has been implemented by an AVR ATtiny2313 (Atmel) 8-bit μC running on a 20-MHz oscillator. The supply voltage of the μC was $V_{\mathrm{DD}} = 5.0$ V, and the resulting voltages were $V_1 = 5.0$ V and $V_{\mathrm{TL}} = 2.2$ V. Pins PD6/ICP (which includes an ST buffer), PB5 and PB7 implemented the function of pins 1, 2, and 3, respectively. The discharging time was measured by the embedded 16-bit Timer 1 with $T_s = 50$ ns. The guidelines indicated in Section III-C to reduce the level of noise were applied.

The circuit in Fig. 2 was tested by measuring a commercial differential capacitive sensor: SCG10Z-G001CC (VTI Technologies), which is a single-axis accelerometer whose main features are summarized in Table II. Its typical values have a tolerance of 20% (or higher), and hence, a measurement system based on this sensor requires a system-level calibration (or field calibration), regardless of the interface circuit used. Such an accelerometer was applied to measure inclination from $-90°$ to $+90°$, which corresponds to $-1g$ to $+1g$ acceleration; according to Table II, such a range of acceleration should move x between -7% and 7%. To know the actual value of inclination (or acceleration) applied, we used as a reference the ADXL103 (Analog Devices). This chip has a single-axis accelerometer and the signal conditioning circuitry, which provides an output voltage proportional to acceleration with a nonlinearity of 0.2% FSS. The ADXL103 was calibrated by means of the gravity ($-1g$ and $+1g$ acceleration). Its bandwidth was set to 10 Hz by an external capacitor of 470 nF, and its output voltage was measured by a digital multimeter (Agilent 34401A).

Since the sensor has a low value of C_0 (Table II), the circuit in Fig. 2 was tested with and without an additional offset capacitor $C_{\mathrm{off},3}$ of 39 pF. Assuming $C_0 = 1.5$ pF, $C_{\mathrm{off},1} = 1$ pF, $C_{\mathrm{off},2} = 2$ pF, and $C_s = 8$ pF, then $k_{s1} = 0.36$ for $C_{\mathrm{off},3} = 0$, whereas $k_{s1} = 0.84$ for $C_{\mathrm{off},3} = 39$ pF, which means that the sensitivity to x should increase by a factor of about 2. The charging resistor R_i was 10 kΩ to have a cutoff frequency (during the charging stage) at least ten times smaller than the operating frequency of the μC [22]. The discharging resistor R_d was 20 MΩ to ensure, from (13), an NLE_q of 1% FSS for $k_{s1} = 0.84$. The measurements were performed at room temperature.

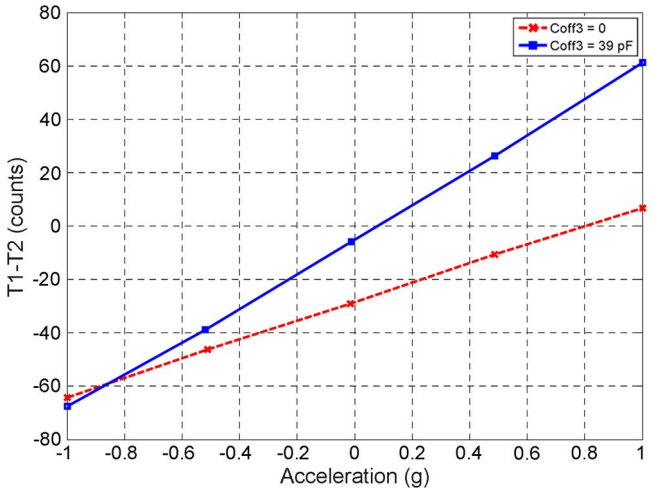

Fig. 6. Experimental results of the difference $T_1 - T_2$ versus acceleration for $C_{\text{off},3} = 0$ pF and $C_{\text{off},3} = 39$ pF.

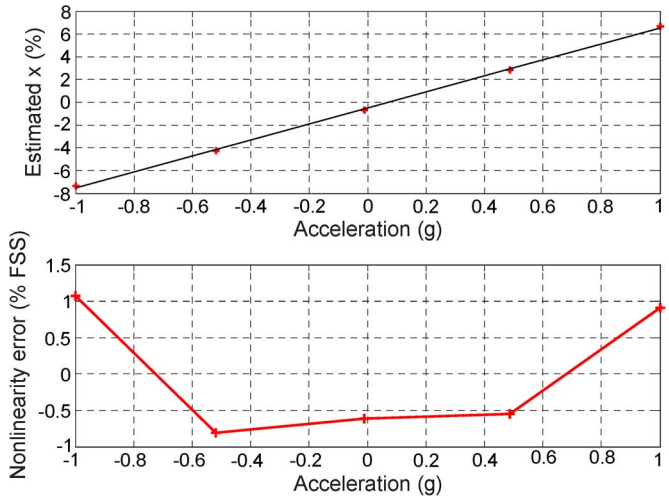

Fig. 7. Experimental results of the linearity test of the interface circuit in Fig. 2 when measuring a single-axis accelerometer and $C_{\text{off},3} = 39$ pF.

V. Experimental Results and Discussion

Fig. 6 shows the difference $T_1 - T_2$ for different values of acceleration applied. This difference increased with the acceleration; however, its sensitivity depended on whether $C_{\text{off},3}$ was used or not, as predicted in (8). The sensitivity for $C_{\text{off},3} = 39$ pF almost doubled that obtained for $C_{\text{off},3} = 0$ pF, which agrees with the theoretical predictions indicated in Section IV. The difference $T_1 - T_2$ was not equal to zero for $0g$ acceleration, which is probably due to the capacitance imbalance of the sensor (Table II), the mismatch of the two additional offset capacitors, and/or the fact that C_{s2} maybe was not exactly equal to C_{s3}. The electronics-level calibration (explained in Section II) is not able to correct this offset error, in part because it is due to the sensor. However, a system-level calibration performed by means of the gravity can easily compensate for this error.

According to Fig. 6, the use of $C_{\text{off},3}$ is appropriate to overcome the loss of sensitivity and, hence, to increase the range of digital numbers (129 for $C_{\text{off},3} = 39$ pF and 71 for $C_{\text{off},3} = 0$ pF). A range of 129 digital numbers provides a resolution of 7 bits (which corresponds to 15 mg) whenever the effects of quantization predominate over those of trigger noise; this seems feasible by averaging ten measurements, which involves an overall measuring time of about 50 ms. This resolution could be improved by the following: 1) increasing the value of R_d, but this involves higher sensitivity to interference due to the high-impedance node; 2) decreasing the value of T_s, which seems practicable in the next future since the speed of microcontrollers is increasing; and 3) using two sensors in parallel, but this of course increases the cost. Anyhow, it seems complicated to achieve a resolution better than 8 bits when the circuit in Fig. 2 is used to measure low-value sensors with low sensitivity.

Fig. 7 shows the resulting x^* [calculated by (10) and averaging 100 values] versus acceleration when $C_{\text{off},3} = 39$ pF. The resulting x^* approximately ranged from -7% to 7%, which is the range expected. Fig. 7 also shows the straight line fitted to the experimental data by means of the least-squares method and the nonlinearity error expressed as a part of FSS. The maximum nonlinearity error was 1.1% FSS, which corresponds to about $0.02g$ and agrees with that expected due to quantization. When the specific IC designed in [6] was used to measure the same sensor, the resolution was 9 bits, and the nonlinearity error was $0.03g$, which are comparable with the results presented herein, although the proposed interface circuit is much simpler.

VI. Conclusion

Using the same approach proposed in a previous work about differential resistive sensors, this paper has shown that differential capacitive sensors can also directly be connected to a general-purpose 8-bit microcontroller without using intermediate electronics between them. The main uncertainty sources of the circuit have been analyzed, and methods to overcome their limitations have been proposed. When those methods are applied, the circuit is able to satisfactorily measure (considering its high simplicity) low-value capacitive sensors with low sensitivity. For example, the measurement of a capacitive accelerometer with $C_0 = 1.5$ pF and $x_{\max} = 7\%$ has shown a nonlinearity error of 1% FSS and a resolution of 7 bits, which can be acceptable for low-cost high-volume applications. Better results are expected when measuring capacitive sensors with a higher value of C_0 and/or higher sensitivity.

Acknowledgment

The authors would like to thank F. López for the technical support and VTI Technologies for providing the sensor samples.

References

[1] L. K. Baxter, *Capacitive Sensors. Design and Applications*. New York: IEEE Press, 1997.
[2] J. Fraden, *Handbook of Modern Sensors: Physics, Designs, and Applications*, 3rd ed. New York: Springer-Verlag, 2004.
[3] R. Pallàs-Areny and J. G. Webster, *Sensors and Signal Conditioning*, 2nd ed. New York: Wiley, 2001.
[4] J. C. Lötters, W. Olthuis, P. H. Veltink, and P. Bergveld, "A sensitive differential capacitance to voltage converter for sensor applications," *IEEE Trans. Instrum. Meas.*, vol. 48, no. 1, pp. 89–96, Feb. 1999.

[5] W. Qu, C. Wenzel, and G. Gerlach, "Fabrication of a 3D differential-capacitive acceleration sensor by UV-LIGA," *Sens. Actuators A, Phys.*, vol. 77, no. 1, pp. 14–20, Sep. 1999.
[6] W. Bracke, P. Merken, R. Puers, and C. Van Hoof, "Ultra-low-power interface chip for autonomous capacitive sensor systems," *IEEE Trans. Circuits Syst. I, Reg. Papers*, vol. 54, no. 1, pp. 130–140, Jan. 2007.
[7] M. Suster, J. Guo, N. Chaimanonart, W. H. Ko, and D. J. Young, "A high-performance MEMS capacitive strain sensing system," *J. Microelectromech. Syst.*, vol. 15, no. 5, pp. 1069–1077, Oct. 2006.
[8] B. George, N. M. Mohan, and V. J. Kumar, "A linear variable differential capacitive transducer for sensing planar angles," *IEEE Trans. Instrum. Meas.*, vol. 57, no. 4, pp. 736–742, Apr. 2008.
[9] F. Han, Z. Gao, and Y. Wang, "A differential capacitance to voltage converter for electrostatic levitation applications," *Sens. Actuators A, Phys.*, vol. 99, no. 3, pp. 249–255, Jun. 2002.
[10] K. Mochizuki, K. Watanabe, T. Masuda, and M. Katsura, "A relaxation-oscillator-based interface for high-accuracy ratiometric signal processing of differential-capacitance transducers," *IEEE Trans. Instrum. Meas.*, vol. 47, no. 1, pp. 11–15, Feb. 1998.
[11] K. Mochizuki, T. Masuda, and K. Watanabe, "An interface circuit for high-accuracy signal processing of differential-capacitance transducers," *IEEE Trans. Instrum. Meas.*, vol. 47, no. 4, pp. 823–827, Aug. 1998.
[12] F. van der Goes, "Low-cost smart sensor interfacing," Ph.D. dissertation, Delft Univ. Technol., Delft, The Netherlands, 1996.
[13] N. M. Mohan and V. J. Kumar, "Novel signal conditioning circuit for push-pull type capacitive transducers," *IEEE Trans. Instrum. Meas.*, vol. 56, no. 1, pp. 153–157, Feb. 2007.
[14] N. M. Mohan, A. R. Shet, S. Kedarnath, and V. J. Kumar, "Digital converter for differential capacitive sensors," *IEEE Trans. Instrum. Meas.*, vol. 57, no. 11, pp. 2576–2581, Nov. 2008.
[15] T. G. Constandinou, J. Georgiou, and C. Toumazou, "Micropower front-end interface for differential-capacitive sensor systems," *Electron. Lett.*, vol. 44, no. 7, pp. 470–472, Mar. 2008.
[16] D. Cox, "Implementing ohmmeter/temperature sensor," Microchip Technol., Chandler, AZ, AN512, 1994.
[17] R. Richey, "Resistance and capacitance meter using a PIC16C622," Microchip Technol., Chandler, AZ, AN611, 1997.
[18] F. Reverter and R. Pallàs-Areny, *Direct Sensor-to-Microcontroller Interface Circuits: Design and Characterisation*. Barcelona, Spain: Marcombo, 2005.
[19] F. Reverter and Ò. Casas, "Interfacing differential resistive sensors to microcontrollers: A direct approach," *IEEE Trans. Instrum. Meas.*, vol. 58, no. 10, pp. 3405–3410, Oct. 2009.
[20] F. Reverter and Ò. Casas, "Direct interface circuit for differential capacitive sensors," in *Proc. IEEE Int. Instrum. Meas. Technol. Conf.*, Victoria, BC, Canada, 2008, pp. 1609–1612.
[21] "Fundamentals of the electronic counters," Hewlett Packard, Palo Alto, CA, Application Note 200, 1997.
[22] F. Reverter, M. Gasulla, and R. Pallàs-Areny, "Analysis of power-supply interference effects on direct sensor-to-microcontroller interfaces," *IEEE Trans. Instrum. Meas.*, vol. 56, no. 1, pp. 171–177, Feb. 2007.
[23] F. Reverter and R. Pallàs-Areny, "Uncertainty reduction techniques in microcontroller-based time measurements," *Sens. Actuators A, Phys.*, vol. 127, no. 1, pp. 74–79, Feb. 2006.

Ferran Reverter was born in Llagostera, Spain, on January 4, 1976. He received the B.Sc. degree in industrial electronic engineering from the University of Girona, Girona, Spain, in 1998, the M.Sc. degree in electronic engineering from the University of Barcelona, Barcelona, Spain, in 2001, and the Ph.D. degree in electronic engineering from the Universitat Politècnica de Catalunya (UPC), Barcelona, Spain, in 2004.

Since 2001, he has been with the UPC, where he is an Associate Professor of analog electronics and digital systems. From 2005 to 2007, he was a Visiting Postdoctoral Fellow with the Delft University of Technology, Delft, The Netherlands. He is the coauthor of the book *Direct Sensor-to-Microcontroller Interface Circuits* (Marcombo, 2005). His research interests are in the field of electronic instrumentation, particularly the design of interface circuits for smart sensors.

Òscar Casas (S'93–A'99–M'05) was born in Barcelona, Spain, on April 15, 1970. He received the M.Sc. and Ph.D. degrees in telecommunication engineering from the Universitat Politècnica de Catalunya (UPC), Barcelona, Spain, in 1994 and 1998, respectively.

He is an Associate Professor of electronic engineering with the UPC and teaches courses in several areas of electronic instrumentation. His research includes sensor interfaces, autonomous sensors, electronic instrumentation, noninvasive physiological measurements, and sensors based on electrical impedance measurements.